NASA TECHNICAL REPORT

NASA TR R-430

HOLOGRAPHIC NONDESTRUCTIVE TESTS PERFORMED ON COMPOSITE SAMPLES OF CERAMIC-EPOXY-FIBERGLASS SANDWICH STRUCTURE

by Robert L. Kurtz and H. K. Liu

George C. Marshall Space Flight Center

Marshall Space Flight Center, Ala. 35812

NATIONAL AERONAUTICS AND SPACE ADMINISTRATION • WASHINGTON, D. C. • JUNE 1974

1. REPORT NO.	2. GOVERNMENT ACCESSION NO.	3. RECIPIENT'S CATALOG NO.
TR R-430		

4. TITLE AND SUBTITLE	5. REPORT DATE
Holographic Nondestructive Tests Performed on Composite Samples of Ceramic-Epoxy-Fiberglass Sandwich Structure *	June 1974
	6. PERFORMING ORGANIZATION CODE
7. AUTHOR(S)	8. PERFORMING ORGANIZATION REPORT #
Robert L. Kurtz and H. K. Liu **	M461
9. PERFORMING ORGANIZATION NAME AND ADDRESS	10. WORK UNIT NO.
George C. Marshall Space Flight Center Marshall Space Flight Center, Alabama 35812	983-15-28-0000
	11. CONTRACT OR GRANT NO.
	13. TYPE OF REPORT & PERIOD COVERED
12. SPONSORING AGENCY NAME AND ADDRESS	Technical Report
National Aeronautics and Space Administration Washington, D.C. 20546	14. SPONSORING AGENCY CODE

15. SUPPLEMENTARY NOTES
Prepared by Space Sciences Laboratory, Science and Engineering. *This work was supported in part by the Pershing Missile System Office Act. Clas. 21X4992.631 63 S01021.
**University of Alabama, Tuscaloosa

16. ABSTRACT

When a hologram storing more than one wave is illuminated with coherent light, the reconstructed wave fronts interfere with each other or with any other phase-related wave front derived from the illuminating source. This multiple wave front comparison is called holographic interferometry, and its application is called holographic nondestructive testing (HNDT).

The theoretical aspects of HNDT techniques and the sensitivity of the holographic system to the geometrical placement of the optical components are briefly discussed. A unique HNDT system which is mobile and possesses variable sensitivity to stress amplitude is described, and experimental evidence of the application of this system to the testing of the hidden debonds in a ceramic-epoxy-fiberglass structure used for sample testing of the radome of the Pershing missile system is presented.

EDITOR'S NOTE

Use of trade names or names of manufacturers in this report does not constitute an official endorsement of such products or manufacturers, either express or implied, by the National Aeronautics and Space Administration or any other agency of the United States government.

17. KEY WORDS	18. DISTRIBUTION STATEMENT
	32

19. SECURITY CLASSIF. (of this report)	20. SECURITY CLASSIF. (of this page)	21. NO. OF PAGES	22. PRICE
Unclassified	Unclassified	31	$3.25

MSFC - Form 3292 (Rev December 1972)

For sale by National Technical Information Service, Springfield, Virginia 22151

TABLE OF CONTENTS

LIST OF ILLUSTRATIONS

FOREWORD

With the advent of modern technology, the need has arisen for components and structures of unprecedented efficiency, the design of which requires that the constituent materials be exploited close to their ultimate capability. Such a design approach requires both a greatly improved understanding and exploitation of the engineering properties of classical materials and the development and use of new materials, such as nonmetallics and composites. With these developments has come the need for commensurate improvements in the HNDT technology.

In response to this need, the Space Sciences Laboratory of the Marshall Space Flight Center designed the Composite Mobile System for Holographic Nondestructive Testing. (This system has patent disclosure number MFS-21704 by the United States Government.) The general purpose of this system is to provide a single system for HNDT which will be mobile and versatile enough to allow any one of the three main nondestructive test methods to be employed.

Recognizing the potential of this system and possessing a very specific need for HNDT of some composite samples of the radome for the Pershing missile system, the Army Missile Command, Redstone Arsenal, Alabama, funded the Space Sciences Laboratory to investigate the composite samples. This simultaneously allowed the further design and development of this unique system for use on Marshall Space Flight Center mainstream programs.

The most recent and present application of this HNDT is in the evaluation of the integrity of electroplate bonds on the Space Shuttle main engine.

HOLOGRAPHIC NONDESTRUCTIVE TESTS PERFORMED ON COMPOSITE SAMPLES OF CERAMIC-EPOXY-FIBERGLASS SANDWICH STRUCTURE

INTRODUCTION

When a hologram storing more than one wave is illuminated with coherent light, the reconstructed wave fronts interfere with each other or with any other phase-related wave front derived from the illuminating source. This multiple wave front comparison is called holographic interferometry, and one application is called holographic nondestructive testing (HNDT). Holographic interferometry, or nondestructive testing, is concerned with the formation and interpretation of the fringe patterns which appear when a wave generated at some earlier time and stored in a hologram is later reconstructed and caused to interfere with a comparison wave. It is this storage or time delay aspect which gives the holographic method a unique advantage over conventional optical interferometry. Holography permits diffusely reflecting or scattering surfaces which are subjected to stress to be interferometrically compared with their nonstressed state. It accomplishes this without the requirement for surface preparation of the test object so necessary for the conventional interferometer.

The purpose of this report is to describe a unique HNDT system which is mobile and possesses variable sensitivity to stress amplitude and to present the experimental evidence of the application of this unique system to the testing of the hidden debonds in a ceramic-epoxy-fiberglass structure used for sample testing of the radome of the Pershing missile system. The theoretical aspects of HNDT techniques and the sensitivity of the holographic system to the geometrical placement of the optical components are briefly discussed.

THEORETICAL DISCUSSION OF RECOGNIZED HOLOGRAPHIC NONDESTRUCTIVE TESTING TECHNIQUES

In any discussion of holographic nondestructive testing it is generally conceded that there are three general types or modes of such testing: real time, double pulse, and time averaged. These will be discussed separately; however, it is submitted here that time-averaged testing is basically not a different type of HNDT but, rather, just a specific loading technique for the other two types. This is a point which should be pursued; however, it will not be pursued further here.

Real-Time HNDT Technique

When the interference of a subject wave with a reference wave is properly recorded in a hologram, a wave whose complex amplitude is linearly proportional to that of the original subject wave can be reconstructed. Reconstruction is best achieved by

placing the hologram plate back in the position it occupied during its exposure and illuminating it with the original reference beam. If it is assumed that the hologram plate has been replaced exactly in its original position, then, apart from a constant amplitude and phase factor, the reconstructed wave will be an exact replica of the original subject wave. (The ratio between the amplitudes of the original and reconstructed waves can be made unity by altering the illumination intensity.) Suppose that during the time between exposure of the hologram and its replacement, while the hologram is being processed, the subject stays fixed in position and continues to be illuminated with laser light. One may now inquire as to what is observed when looking through the replaced hologram in the direction of the subject. Since most holographic interferometry has been carried out using holograms formed in photographic emulsion, assume this to be the case here and recall that the reconstructed wave amplitude will then have a negative sign relative to the original subject wave. Provided that (1) processing of the hologram does not distort the emulsion, (2) the replacement has been exact, and (3) the illumination has been adjusted to equalize the absolute values of the original and reconstructed subject wave amplitudes, the reconstructed wave fronts will cancel the original subject wave fronts at every point on the viewer's side of the hologram. To the viewer looking through the hologram, the subject will, therefore, not be visible. (In practice, at least one broad, bright fringe is usually observed because the processing of the hologram inevitably distorts the emulsion to some small degree.)

If the subject of the hologram is a plane mirror surface, the holographic method described above does no more than can be accomplished with a Michelson interferometer illuminated with uniform coherent light. Because the mirror surfaces can be polished so smooth that any surface microstructure is of negligible consequence, one good mirror surface is the equivalent of another. By means of the beam splitter in the Michelson instrument, a given mirror surface can be interferometrically compared with its equivalent. Totally destructive or constructive interference can be observed as with the holographic method.

It is, however, the unique property of the holographic method that an arbitrarily shaped, rough scattering surface with complex microstructure can be interferometrically compared to another similar surface with no more difficulty (in principle) than is encountered with polished mirrors. The virtual image of a diffusely scattering subject generated by the hologram may be considered to provide one such surface. The other is the actual subject surface itself. If the original reference wave illuminates an exactly replaced hologram, the virtual image will appear to the viewer to be not only a macroscopic replica of the subject, but to lie coincident with it in space and to bear a surface microstructure whose light-scattering properties are identical to those of the subject. It would be a formidable task to attempt to replace the two mirrors of the Michelson interferometer with two such identical physical surfaces. Holography in effect does this.

Once an effective coincidence of the virtual image with the subject is achieved, the latter may be placed under stress and caused to deform, or it may be released from stress and allowed to flow, creep, deflate, or expand. As a result, the optical distance

from an observation point to any point of the displaced surface will change relative to its distance to the corresponding point on the comparison surface (that of the virtual image). Distances of surface points from the light source, which in effect illuminates both surfaces, also change. Accordingly, coherent light rays scattering from identical but displaced surface areas (areas with identical microstructure) will acquire a relative phase shift in transit from source to observation plane. The phase shift and the consequent wave-amplitude addition and subtraction which lead to the observed fringe pattern are characteristic of the subject surface deformation. As a change in the subject surface occurs, a change in the fringe pattern can be simultaneously observed – hence the name real-time holographic interferometry. It is axiomatic that the stress-induced deformations must not appreciably alter the surface microstructure. Since a rough surface acts as a random scatterer, any significant alteration of the roughness of the surface would impose a new random phase distribution on the light wave reflected from the subject. The subject wave and the reconstructed subject wave would then form a high spatial frequency interference pattern no longer interpretable in terms of the low spatial frequency surface deformations of interest.

Several factors tend to add to the difficulty of real-time holographic interferometry. If the fringe pattern is to be observed at all or if it is to be characteristic of the intended displacement, the subject position and its illumination at the time when the processed hologram is replaced must be identical to that when the hologram was formed. This generally implies that the subject and the optical components required to form the hologram either must be kept fixed in position during the intervening period between exposure and observation or must be capable of being returned to their original positions with great accuracy. One must register the fringe pattern formed by the subject and reference beams at the time of observation with that recorded in the hologram to within a small fraction of a fringe spacing. The task is easier when subject-to-reference beam angles are small. An additional complication is the emulsion shrinkage accompanying the wet processing of photographic plates. This causes some unavoidable distortion of the reconstructed wave fronts and, thereby, a distortion of the regularity of the observed interference fringes. Moreover, until the plate is thoroughly dry, continuing shrinkage may confuse attempts to register the hologram with the original reference beam.

Despite such impedimenta, it is possible to obtain high-contrast fringes. Real-time interferometry offers a distinct advantage in that it is capable of continuously monitoring displacements of a rough surface without touching or marking the surface (as, e.g., in moire techniques). A secondary, but useful, advantage over double-exposure methods is the freedom allowed by the real-time method to make small adjustments of the hologram plate that can optimize the fringe display for quantitative interpretation.

The theoretical description of real-time HNDT or stored-beam interferometry is presented from the point of view of Reference 1. When looking through the hologram at the object, an observer will see two images. One is the reconstructed image; the second is the illuminated object itself. The amplitude of the light formed by the hologram is

$$-k_{rr}^{*}\, S_o \quad . \qquad (1)$$

The object scatters light denoted by S . The amplitudes sum, resulting in an amplitude

$$A = S - krr^* So \quad . \tag{2}$$

The eye integrates the intensity, resulting in

$$I_r = \int |S - krr^* So|^2 \, dt \quad . \tag{3}$$

The loading of the object must now be considered and related to the scattering, S , and the stationary amplitude, So [1].

Double-Exposure HNDT Technique

Continuous comparison of surface displacement relative to an initial state may in certain cases supply more information than is necessary. If it is sufficient to form a permanent record of the relative surface displacement occurring after a fixed interval of time, a method obviating the experimental difficulties of real-time interferometry may be employed. Two exposures of the hologram, once to the initial state of the surface and once to its strained state, are superimposed prior to processing. Each exposure is made with the identical reference wave. With this double-exposure, or time-lapse method, the problems of registering a reconstructed wave with an original are eliminated. After the exposure of the hologram is completed, the subject and the optical components used to illuminate the subject are no longer of concern. Both the comparison wave, characteristic of the surface in its initial state, and the wave representing a later, altered state of the surface are reconstructed in register by illuminating the hologram with a wave similar to the original reference wave. No more care in illumination is necessary than is taken in illuminating any pictorial hologram. Distortion due to emulsion shrinkage is identical for both reconstructed waves and is, therefore, not a factor in determining the spacing of the fringes formed by the interference of the two waves. However, limitations on the change of subject surface microstructure apply here as in the real-time method.

Illumination of the doubly exposed hologram not only effects the simultaneous reconstruction of two waves which had been scattered from the subject at different times but causes them to interfere under ideal conditions. The waves can share the diffraction efficiency of the hologram equally. Thus, their intensities are equal and the intereference fringes they produce can have high visibility or contrast. For purposes of analysis, the two virtual images of the subject surface generated by the reconstructed waves may be considered to be two slightly different physical surfaces. One can imagine these

initial-state and final-state surfaces to be simultaneously illuminated with the coherent light originally illuminating the subject. One difference in the interference resulting from the double-exposure method as compared to that obtained from the real-time technique may be observed when initial and final states of the subject surface are identical. Each reconstructed wave is negative with respect to the original subject wave; and, consequently, when the initial and final states are identical, the reconstructed waves add to give a bright image of the subject.

Suppose a hologram was made of an object having a scene beam amplitude S_1. If the object is strained and a second exposure made corresponding to scene beam amplitude S_2 on the same hologram, upon reconstruction, two virtual images will be seen when viewing through the hologram. Their composite amplitude is given by

$$A = -krr^* (S_1 + S_2) \quad . \tag{4}$$

These two scene beams will interfere with each other constructively or destructively, depending on their relative phase. Areas of destructive interference will cause fringes (absence of light). The intensity of the composite image, I_T, is given by $|A|^2$ or

$$I_T = |A|^2 = (krr^*)^2 (S_1 + S_2)(S_1^* + S_2^*) \quad . \tag{5}$$

The two scene beam amplitudes, S_1 and S_2, can be related by simple geometry. Let $\ell_1 + \ell_2$ be the path of light taken by the scene beam when the film is exposed to the unstrained object. Similarly, $\ell'_1 + \ell'_2$ is the path length of the scene beam when the second exposure is made. Then, referring to Figure 1,

$$\ell'^2_1 = \ell_1^2 + m^2 - 2m\ell_1 \cos\theta_1 \quad ,$$

$$\ell'^2_2 = \ell_2^2 + m^2 - 2m\ell_2 \cos\theta_2 \quad .$$

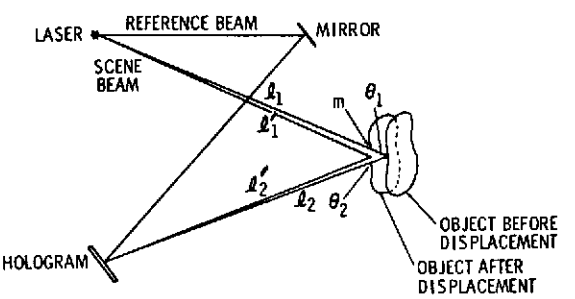

Figure 1. Phase change of light due to the movement of the object.

Solving for ℓ'_1 and ℓ'_2,

$$\ell'_1 = \ell_1\left[1 + \left(\frac{m}{\ell_1}\right)^2 - \frac{2m}{\ell_1}\cos\theta_1\right]^{1/2} \cong \ell_1\left(1 - \frac{m}{\ell_1}\cos\theta_1\right) \text{ for } \frac{m}{\ell_1} \ll 1 \quad ,$$

$$\ell'_2 = \ell_2\left[1 + \left(\frac{m}{\ell_2}\right)^2 - \frac{2m}{\ell_2}\cos\theta_2\right]^{1/2} \cong \ell_2\left(1 - \frac{m}{\ell_2}\cos\theta_2\right) \text{ for } \frac{m}{\ell_2} \ll 1 \quad .$$

Therefore,

$$\ell'_1 - \ell_1 = -m \cos\theta_1 \qquad \text{or} \qquad \ell_1 - \ell'_1 = m \cos\theta_1 \quad ,$$

$$\ell'_2 - \ell_2 = -m \cos\theta_2 \qquad \text{or} \qquad \ell_2 - \ell'_2 = m \cos\theta_2 \quad .$$

Total pathlength change is determined by

$$\Delta L = (\ell_1 + \ell_2) - (\ell'_1 + \ell'_2) = m(\cos\theta_1 + \cos\theta_2) \quad .$$

The difference in phase is given by

$$\Delta\phi = \frac{2\pi}{\lambda} \Delta L = \frac{2\pi}{\lambda} m (\cos\theta_1 + \cos\theta_2) \quad . \tag{6}$$

The scene beam, S_1 , during the first exposure is given by

$$S_1 = S e^{i\phi} \quad ,$$

and the scene beam, S_2 , during the second exposure is given by

$$S_2 = S e^{i\phi} + \frac{2\pi i}{\lambda} m(\cos\theta_1 + \cos\theta_2) \quad , \tag{7}$$

$$S_2 = S_1 e \frac{2\pi i}{\lambda} m(\cos\theta_1 + \cos\theta_2) \quad . \tag{8}$$

Then equation (5) becomes

$$I_r = (krr^*)^2 \; S_1 S_2^* \left| 1 + e^{\frac{2\pi i}{\lambda} m(\cos\theta_1 + \cos\theta_2)} \right|^2$$

$$= (krr^*)^2 \; |s|^2 \left\{ 2 + 2\cos\left[\frac{2\pi}{\lambda} m(\cos\theta_1 + \cos\theta_2) \right] \right\}$$

$$= 2k^2 \; |r|^4 \; |s|^2 \left\{ 1 + \cos\left[\frac{2\pi}{\lambda} m(\cos\theta_1 + \cos\theta_2) \right] \right\} \quad . \tag{9}$$

Note that the intensity given by equation (9) has zeros indicating the presence of fringes, namely, when

$$1 + \cos\left[\frac{2\pi}{\lambda} m(\cos\theta_1 + \cos\theta_2) \right] = 0 \quad ,$$

or

$$\frac{2\pi}{\lambda} (\cos\theta_1 + \cos\theta_2) m = (2n - 1)\pi \quad , \qquad n = 1, 2, 3 \ldots , \tag{10}$$

or

$$m = \frac{2n - 1}{2(\cos\theta_1 + \cos\theta_2)} \lambda \quad . \tag{11}$$

If $\theta_1 = \theta_2 = 0$, that is, normal incidence and reflection of the illuminating light and normal displacement, then

$$m = \frac{2n - 1}{4} \lambda \quad . \tag{12}$$

This says that a fringe will be formed when the body moves an odd number of quarter wavelengths between exposures.

Time-Averaged HNDT Technique

The method for forming a time-averaged hologram of a vibrating surface is identical to that used for forming a hologram when a surface is stationary. If the maximum amplitude of the vibration is limited to some 10's of light wavelengths, illumination of the hologram yields an image of the surface on which is superimposed a number of observable interference fringes. It should be emphasized that these fringes are contour lines of equal displacement of the surface. Whereas a few of these may be nodal contours, most are contours of equal displacement plotted on the moving regions of the surface.

To illustrate a relation between vibration amplitude and the intensity of the fringe pattern, consider a vibrating membrane illuminated with parallel coherent light as in Figure 2. When the membrane surface is static, it is assumed to lie in the x-z plane, and its displacement from that plane during vibration is assumed to be suitably small. A clamp at the outer edges of the surface fixes one nodal contour. The arrangement so analyzed is similar to the case of pure rotation illustrated in Figure 15.5 of Reference 2. In the present case, consider the displacement $AA' = D(x,t)$ at some instant of time, t. If simple harmonic motion is assumed, then the displacement of an arbitrary point at time t may be written as

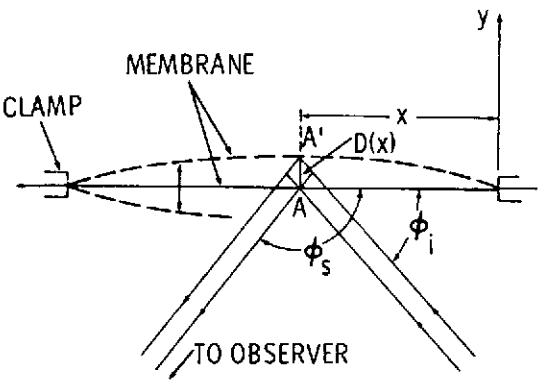

Figure 2. Geometry for calculating the phase shift $\delta(x,t)$ for the time-averaged method.

$$D(x,t) = D(x) \cos \omega t \quad , \tag{13}$$

where ω is the angular frequency of vibration. By substituting $D(x,t)$ for $x\alpha$ in the first equation below, one obtains for the instantaneous phase shift of the scattered rays

$$\delta(x,t) = -(2\pi/\lambda)(x\alpha)(\sin \phi_i + \sin \phi_s)$$

$$\delta(x,t) = -(2\pi/\lambda)\, D(x) \cos \omega t\, (\sin \phi_i + \sin \phi_s) \quad . \tag{14}$$

Before $\delta(x,t)$ can be used to calculate the intensity to the fringe pattern, the hologram recording process must be considered. One must insure that the hologram records a time-average of the interference pattern intensity produced by the

time-dependent subject complex amplitude at the hologram plane. In practice this means that the exposure time should be long compared to the vibration period; in the present calculation, however, one can average over exactly one period of vibration.

To form a hologram of a vibrating surface, a photosensitive medium is exposed to a reference plane wave whose complex amplitude at the hologram plane is r and to subject waves reflected from the vibrating surface to the hologram plane with a complex amplitude $S(x,t)$. The subject wave complex amplitude is a function not only of the spatial coordinate x but also of the t. At any time, t, the intensity at the hologram is

$$I(x,t) = S(x,t)\,S^*(x,t) + r^2 + S^*(x,t)r + S(x,t)r^* \tag{15}$$

where $r = |r|$. The exposure of the hologram is proportional to the time-average of $I(x,t)$

$$\langle I \rangle = \frac{1}{T} \int_0^T I(x,t)dt \tag{16}$$

where $T = 2\pi/\omega$ is the vibration period of the surface and ω is the angular frequency. By substituting for $I(x,t)$ from equation (15), equation (16) may be written as

$$\langle I \rangle = \frac{1}{T} \int_0^T [S(x,t)\,S^*(x,t) + r^2 + S^*(x,t)r]\,dt + \frac{r^*}{T} \int_0^T S(x,t)dt \tag{17}$$

where the term of interest is separated, at the far right. This last term leads to a reconstruction of the original subject wave and a virtual image of the subject surface. If a plane absorption hologram is exposed and processed so that it is a linear recording of the subject wave, then its amplitude transmittance is proportional to $\langle I \rangle$. Illumination by the original reference wave reconstructs the time-averaged original subject wave given by the product

$$\begin{aligned} w &\propto r \cdot \frac{r^*}{T} \int_0^T S(x,t)dt \\ &\propto \frac{1}{T} \int_0^T S(x,t)dt \; \frac{1}{2\pi} \int_0^{2\pi} S(x,t)\,d(\omega t) \quad . \end{aligned} \tag{18}$$

The mathematical form of equation (17) holds for the light coming from any subject point and for the wave front of the subject light at an arbitrary distance from the subject. Suppose a(x,t) represents the instantaneous complex amplitude of the light arriving at an observation point P from a point A on the vibrating surface. One may write a(x,t) as

$$a(x,t) = a(x) \exp[i\delta(x,t)] \tag{19}$$

where a(x) is the complex amplitude at P when the vibrating surface lies in the x-z plane and where $\delta(x,t)$ [given in equation (14)] is the extra phase difference produced by the displacement of the surface D(x,t). If a(x,t) is substituted for S(x,t) in equation (18), the complex amplitude of the reconstruction of the wave originally traveling from A to P may be written as

$$w_A \alpha\, a(x) = \int_0^{2\pi} \exp[i\delta(x,t)]\, d(\omega t) \quad , \tag{20}$$

The integral in equation (20) presents interference at the point P of light from the undisplaced point A with that from corresponding points A′, A″, etc., where the latter are all the displaced positions of A produced by the vibration. By substituting $\delta(x,t)$ from equation (14) into equation (20), one can evaluate the factor modulating the complex amplitude a(x) of the wave coming from the undisplaced surface. Thus,

$$\frac{1}{2\pi} \int_0^{2\pi} \exp[i\delta(x,t)]\, d(\omega t)$$

$$= \frac{1}{2\pi} \int_0^{2\pi} \exp\left[-i \frac{2\pi}{\lambda} D(x) \cdot (\sin \phi_i + \sin \phi_s) \cos \omega t\right] d(\omega t)$$

$$= J_o\left[\frac{2\pi}{\lambda} D(x) \cdot (\sin \phi_i + \sin \phi_s)\right]$$

where J_0 is the zero-order Bessel function of argument $(2\pi/\lambda)D(x) \cdot (\sin \phi_i + \sin \phi_s)$. The intensity at the observation point is

$$w_A w_A^* \propto a(x)\, a^*(x) \left\{ J_0 \left[\frac{2\pi}{\lambda} D(x) \cdot (\sin \phi_i + \sin \phi_s) \right] \right\}^2 \quad . \tag{21}$$

Equation (21) indicates that the dark fringes in the observed interference pattern of a sinusoidally vibrating surface correspond to the zeros of the J_0^2 function, and the bright fringes correspond to the maxima of the function. These maxima decrease with increasing values of the argument with increasing displacement amplitude D(x). The fall-off of intensity limits the number of fringes which have sufficient visibility to be seen by an observer.

Time-averaged holography enables the vibrational amplitudes of diffusely reflecting surfaces to be measured with interferometric precision. It eliminates the need to place sensing elements of any sort in contact with the vibrating surface. Curvature of the surface is not a factor as it is when Chladni patterns are employed. The method has been applied to the study of a variety of vibrating objects ranging from quartz crystals to treble-viol plates and can yield greater detail about the antinodal region than previous techniques. There are, however, limitations which have prompted an investigation of other means to extend holography to the study of vibrating objects. One of these limitations, the diminution in fringe visibility as the vibration amplitude increases, has already been cited. Another is that the relative phase of the vibration is not given by the measurement.

DEPENDENCE OF HOLOGRAPHIC SENSITIVITY ON THE GEOMETRY OF OPTICAL COMPONENTS

Because holography is an interference phenomenon, the total change in path length, Δd, of the object beam during the exposure must be less than $\lambda/2$ (i.e., $k\, 2\pi/\lambda = \pi$). Due to this severe restriction, the geometry of the optical arrangement employed becomes of utmost importance to the successful recording of a moving object or particle. Therefore, attention is directed to two limiting cases of sideband geometry.

Consider the holographic arrangement of Figure 3. This constitutes a very desirable arrangement for a stationary object because of the high energy return from the object to the film plate. For this case, the radiation propagation vector $\vec{K}$ is both parallel and antiparallel to the direction of the intended object motion, Δx. Consider that during the exposure the object moves from position x_0 to a new position x_1; the object translation is Δx. Then the total optical path length change is

$$\Delta d = 2\Delta x \quad ;$$

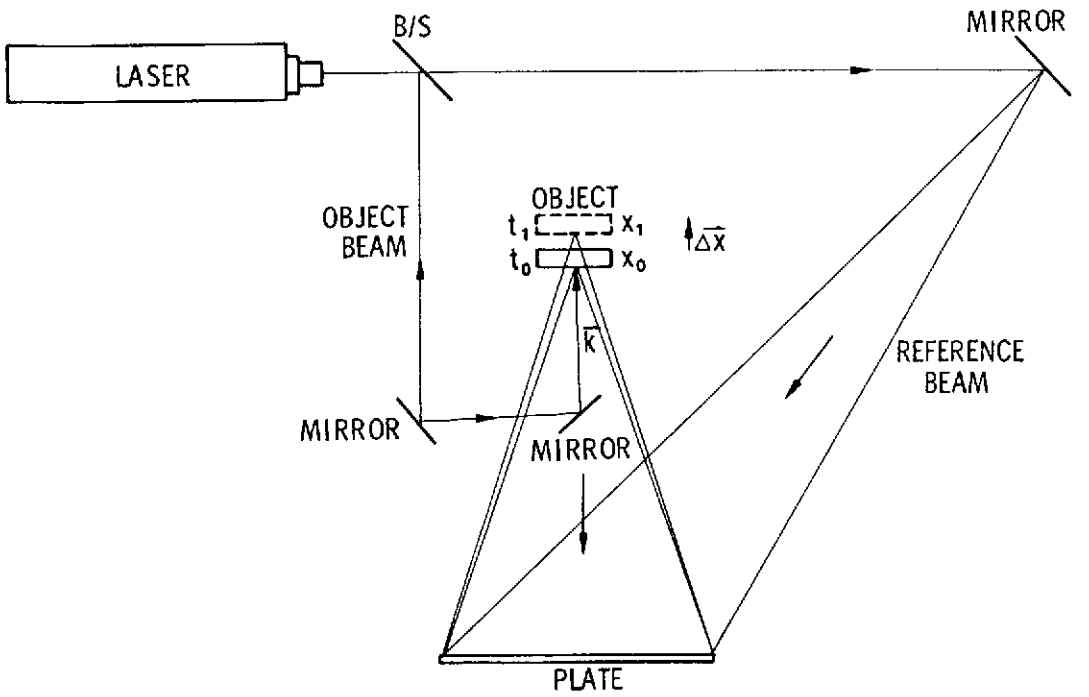

Figure 3. Minimum motion geometry.

yet, using the limiting requirement for the allowed change in optical path length of a holographic arrangement,

$$2\Delta x < \lambda/2$$

or

$$\Delta x < \lambda/4 \quad ,$$

and the object cannot travel a total distance greater than $\lambda/4$ if one is to successfully record a hologram. This was an obvious result when the object motion, Δx , was allowed to be along the direction of the radiation propagation vector, $\vec{k}$. This geometry allows the minimum object motion during the exposure.

A contrasting case is afforded by Figure 4. The basic difference in geometry between this and the previous arrangement is the rotation of one mirror. Everything is as before except that now the direction of motion, Δx , of the object is perpendicular to

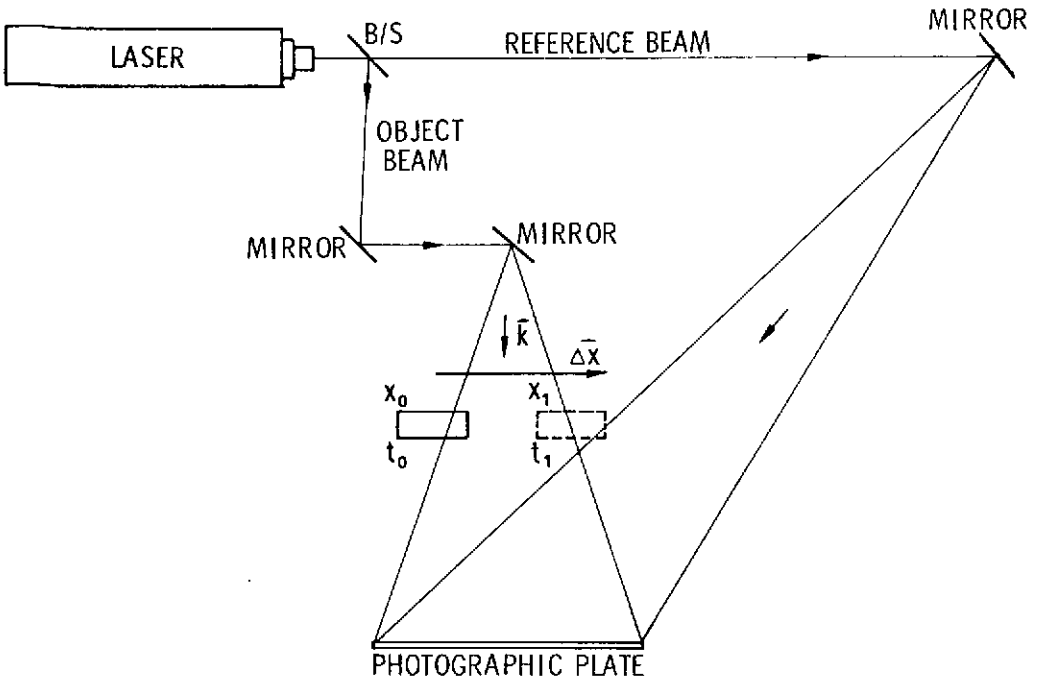

Figure 4. Maximum motion geometry.

the propagation vector $\vec{k}$. The result is, of course, that now the magnitude of Δx may be as large as desired without any change occurring in the object beam path length. For this geometrical arrangement then

$$\Delta d \equiv 0 \quad .$$

Of course, if one expects to resolve the object in the hologram with such an arrangement, the allowed Δx is not totally unlimited. As a rule of thumb, it may not travel further than one-tenth of its length during the exposure due to resolution requirements. But this is an unusually large distance compared to $\lambda/2$. The price paid for this large motion is that no resolution of front surface detail has been recorded. The image simply appears as a black silhouette against a lighted background.

Because the sensitivity of holography is a function of the geometry employed for the optical components, a unique HNDT system with variable sensitivity has been devised which allows any form of loading, i.e., change in subject amplitude as a result of loading. This is accomplished by proper selection of geometry which allows minimum change in optical components to control the expected sensitivity. This system will be described in the following section.

DESCRIPTION OF A COMPOSITE MOBILE HOLOGRAPHIC NONDESTRUCTIVE TESTING TECHNIQUE – A VARIABLE SENSITIVITY SYSTEM

Using a variable sensitivity system, all methods of HNDT can be accommodated with basically the same holographic arrangement. Attention is directed to Figure 5. Configuration No. 1 may be described as follows: Radiation emitted from the laser is incident on the field mirror assembly which contains a spatial filter and essentially a beam splitter. This assembly or unit is translatable to the left along the path ΔSb . The reflected portion of the radiation is made incident on the micrometer translatable object in such a direction as to make an angle $\theta = 0$ with the perpendicular bisector of this object. This radiation is then turned antiparallel to itself where it passes on to the film recorder. The film recorder is itself translatable to the right along the path Δf .

The radiation transmitted through the field mirror assembly is incident on mirror M , which is itself translatable to the right along path Δm . From here it is turned to be incident on the film recorder and interferes with the object beam.

Configuration No. 2 may be traced in a similar fashion, except that the object beam makes some angle $\theta > 0$ with the perpendicular bisector of the object.

The system is composite because ones needs to only slightly manipulate three components (field mirror assembly, mirror M , and film recorder) to change from one method of HNDT to another. It is not necessary to establish a new geometry in order to perform the various HNDT methods. The system is mobile because all of the optical components are mounted on a precalibrated rigid table and may be locked in any position along their translatable paths. The system has variable sensitivity (which affords the composite structure) by virtue of the control over the angle θ which the object beam makes with the perpendicular bisector of the object.

Attention is directed to equation (11) of the double-exposure technique where it was shown that zeros indicating the presence of fringes occur for

$$m = \frac{2n - 1}{2(\cos\theta_i + \cos\theta_s)} \lambda \quad .$$

Consider the case of $\theta_1 = \theta_2 = 0$, $\lambda = 5145\text{Å}$; then equation (11) becomes

$$m = (2n - 1)\frac{\lambda}{4} = (2n - 1)\frac{5145\text{Å}}{4}$$

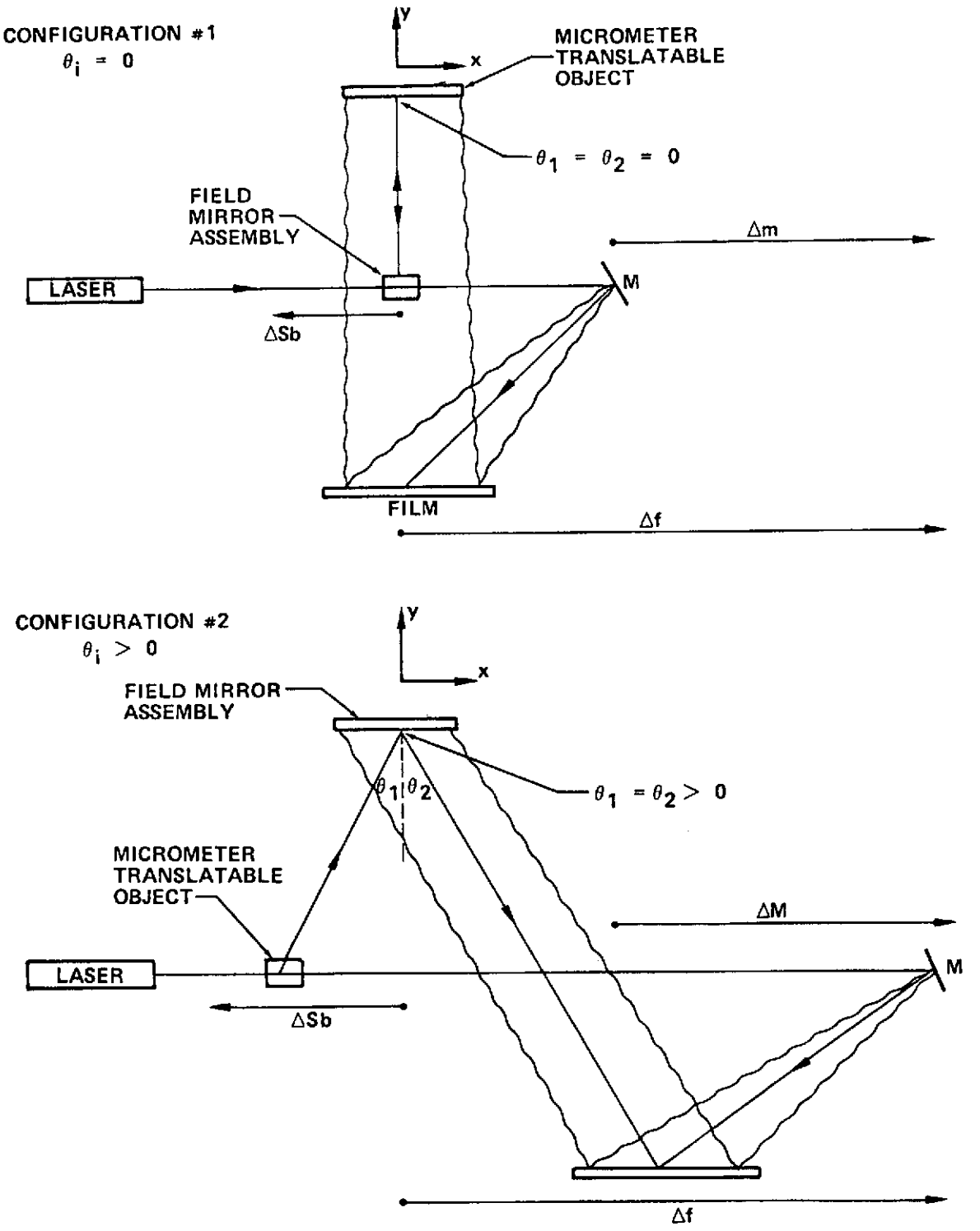

Figure 5. Composite mobile holographic nondestructive test system.

which says that the movement of the object (parallel or antiparallel to the k vector) of 0.1286 μm will be sufficient to cause one fringe to appear on the object.

On the other hand, consider the case of $\theta_1 = \theta_2 = 75$ deg and, again, $\lambda = 5145\text{Å}$; then equation (11) becomes

$$m = (2n - 1)\frac{\lambda}{1.0353} = (2n - 1)\frac{5145\text{Å}}{1.353}$$

which says that in order to obtain one fringe on the object the movement of the object (in the same direction) must be as great as 0.4970 μm. While both of these movements are small, their relative values differ by about one-half order of magnitude. This provides an indication of the variation of sensitivity of this system by the minute adjustment of three single components on a precalibrated mobile table. The table is precalibrated in terms of the desired sensitivity.

Figure 6 shows the result of movement along the k vector for the two configurations of the system. For both configurations, the translation of the object is along the negative z direction (see Figure 5).

EXPERIMENTAL RESULTS

The composite mobile holographic technique was applied to several sandwich-structured samples of the radome of the Pershing missile system in which some specific programmed flaws had been placed. The technique was applied to determine and locate these flaws in order to develop a confidence in this technique as a possible candidate for use as a testing technique on the radome itself.

The Test Samples

The test samples were fiberglass-epoxy-ceramic sandwich structures as illustrated in Figure 7. Three kinds of flaws, or debonds, were programmed into the structure; the locations of these are represented by the dashed lines of Figure 7. Three test samples, 15.24 cm X 15.24 cm (6 in. X 6 in.), were provided for these tests. Figure 8 is a photograph showing the fiberglass side, the ceramic side, and one edge. Common to the three samples, called plates 1, 2, and 3, respectively, was an AF-32 plug which was formed and precured prior to installation into the epoxy layer of the sandwiched structure. Plates 1 and 2 had fingerprints of grease at the epoxy-ceramic interface, and

$\theta_1 = \theta_2 = 0 \quad \Delta d = 0.1286\ \mu m$

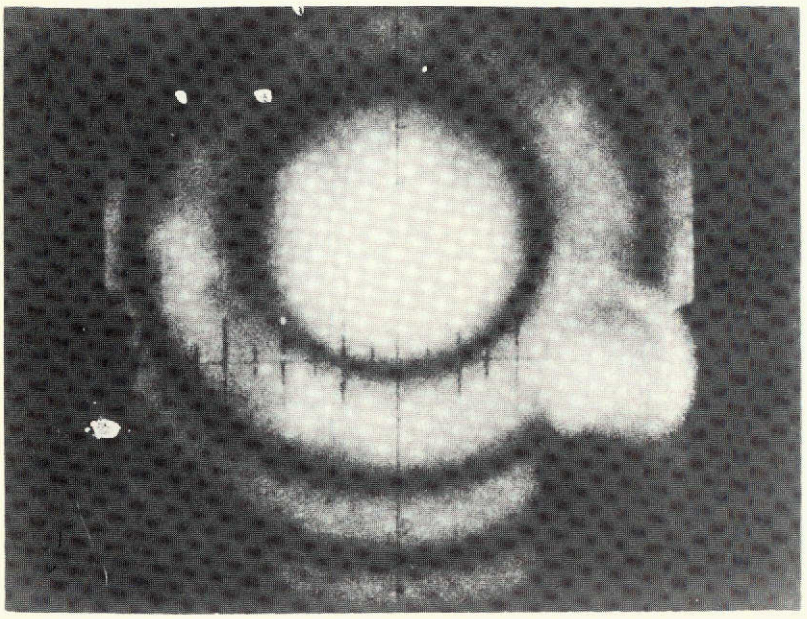

$\Delta z = 0$

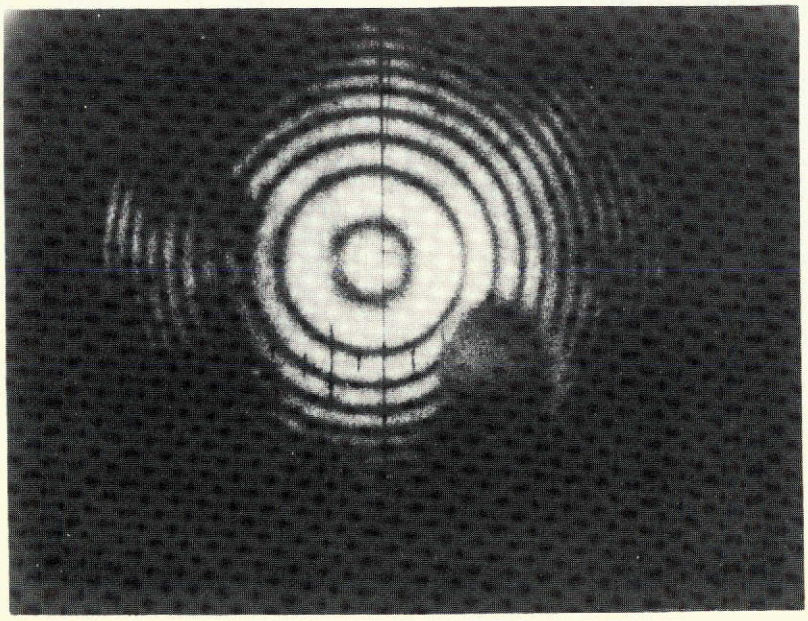

$\Delta z = 0$

Figure 6. Results of controlled object movement.

$\theta_1 = \theta_2 = 15$ deg $\Delta d = 1.333\ \mu m$

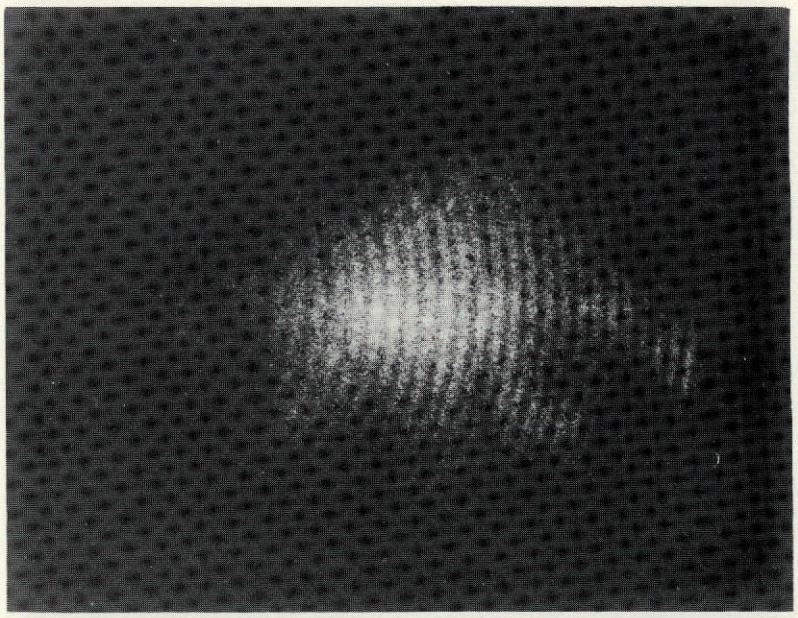

$\Delta z = 1.5\ \mu m$

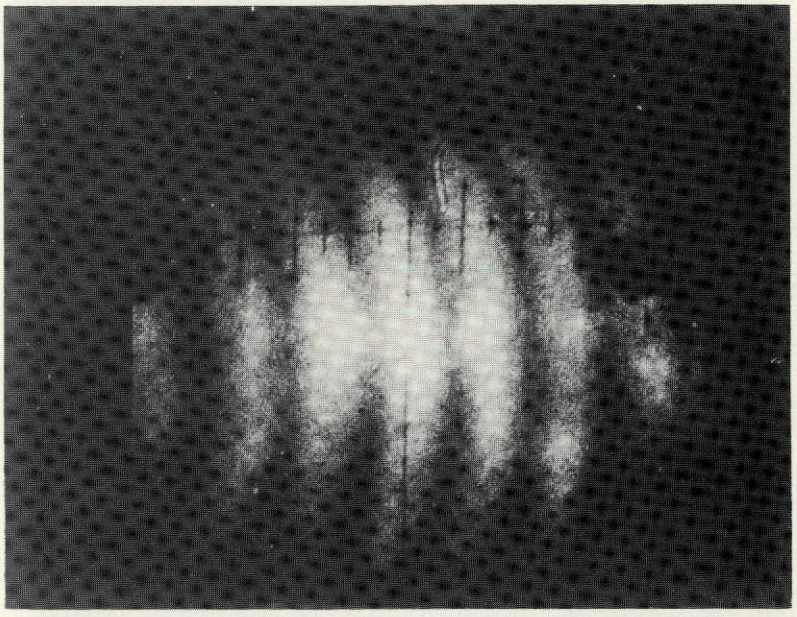

$\Delta z = 0.25\ \mu m$

Figure 6. (Concluded).

the same type of fingerprints were placed at the fiberglass-epoxy interface on plate 3. The area location of the 2.54-cm diameter Teflon disc was identical for all three plates, yet the interface position was different for all three. The disc was placed at the fiberglass-epoxy interface on plate 1, at the ceramic-epoxy interface for plate 2, and in the middle of four plies of epoxy for plate 3.

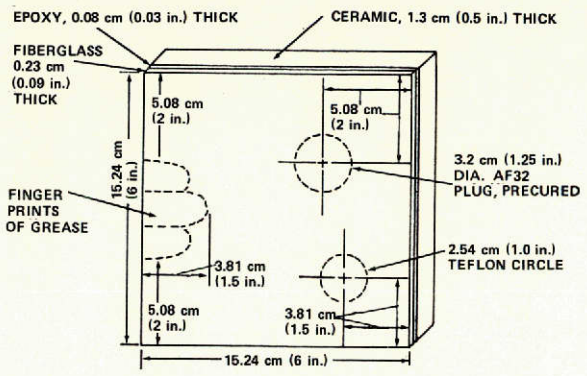

Figure 7. The structure of test samples.

The physical characteristics of the sample components and programmed flaws are described as follows:

The ceramic material employed for the sandwich structures tested was a high purity, slip-cast fused silica (SiO_2). It is a noncrystalline or amorphous material obtained from melting any of the crystalline forms of silica. Its density is about 3.75 gm/cm^3 (234 lb/ft^3) and its softening point is 1729°C (3144°F). The tensile strength of the material ranges from 1.33 X 10^7 dyne/cm^2 (6 X 10^3 psi) to 2.2 X 10^7 dyne/cm^2 (10^4 psi) in the temperature range 93 to 538°C (200 to 1000°F). The compressive strength in the corresponding temperature range is an order of magnitude higher than the tensile strength. The thermal conductivity is approximately 4.2 X 10^{-3} cal/cm-sec-°C (0.5 BTU/ft-hr-°F), with a specific heat of 0.18 cal/gm-°C (0.18 BTU/lb-°F) and a flexural strength of 1.08 dyne/cm^2 (6.5 X 10^3 psi).

An S fiberglass was used which consisted of eight layers of glass cloth held together by 30 to 33 percent epoxy resin (ERL epoxy 2256-tonox 6040). It had a

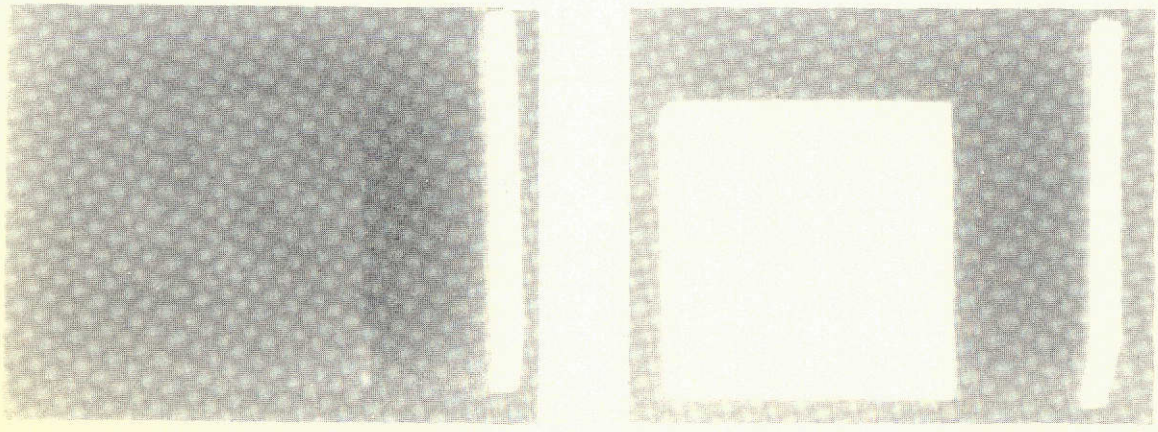

Figure 8. Photograph of test samples.

thermal conductivity of 0.198 cal/gm-°C (0.198 BTU/lb-°F) and a density of 1.76 gm/cm^3 (110 lb/ft^3). The fiberglass and ceramic were bonded together by the AF-32 epoxy (3M Company). The thermal conductivity of this epoxy was 2.94 X 10^{-3} cal/cm-sec-°C (0.35 BTU/ft-hr-°F), the specific heat was 0.45 cal/gm-°C (0.45 BTU/lb-°F), and the density was 1.52 gm/cm^3 (95 lb/ft^3). Four plies of the epoxy were used, resulting in a total thickness of 0.2286 cm (0.09 in.).

The Sample Holder

A schematic of the sample holder, for the positive pressure loading, is shown in Figure 9. The test sample is clamped from the front by a set of eight set screws; then positive gas pressure is applied from the air inlet located in the center of the holder back. Because of the positive air pressure acting on the "O" ring, all leaks are sealed and a positive pressure may be maintained for a reasonable time. Photographs showing the front and rear views of the holder are presented in Figure 10.

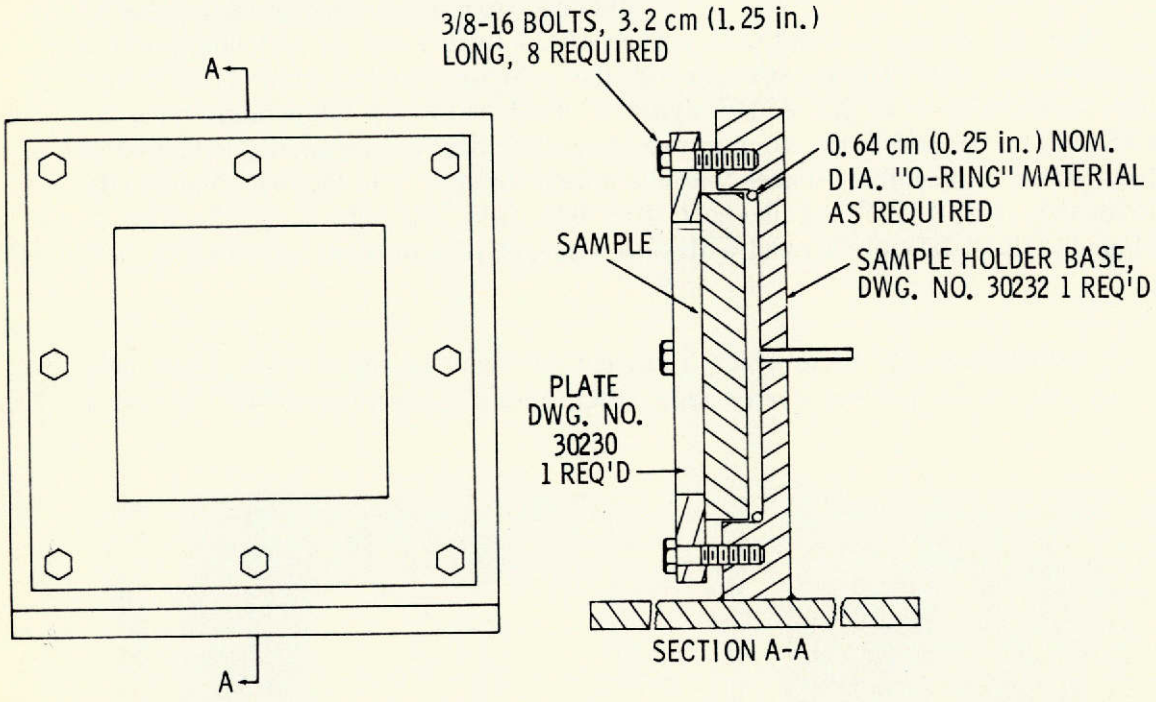

Figure 9. Sample holder assembly schematic.

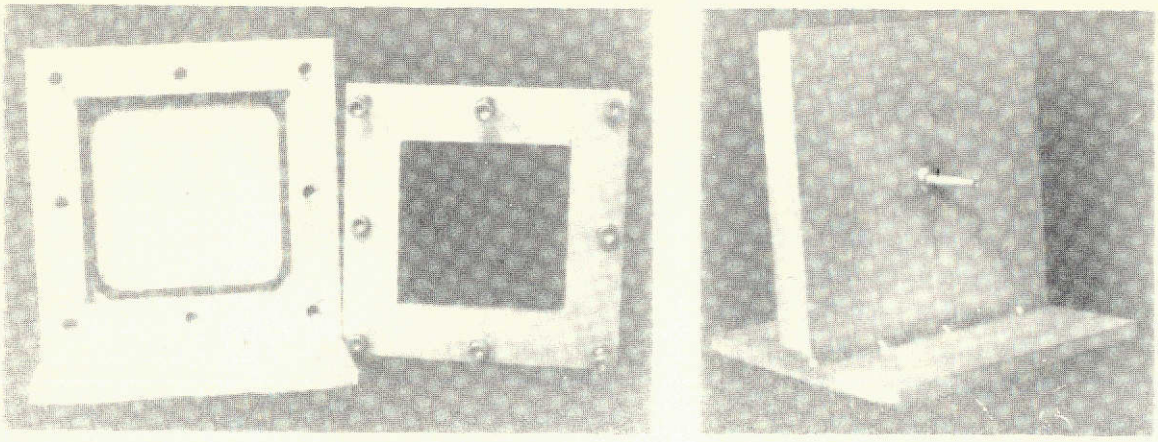

a. Front view. b. Rear view.

Figure 10. Photograph of sample holder.

The Experimental Procedure

The experimental procedure for this testing consisted of the following steps:

1. Loading a test sample in the holder, checking for pressure leaks, and placing this holder properly in the holographic system.

2. Obtaining a reference hologram of the test sample and accurately replacing this hologram back into position in the holographic system such that the virtual image of the reference hologram was superimposed on the real test object.

3. Observing the interference pattern for sequential continuous changes in the positive pressure loading.

4. Recording the fringe variations by taking photographs of the virtual image through the hologram.

These steps constitute the real-time observation of the fringe pattern (real-time interferometry) and the search mode necessary to determine if the loading technique employed is adequate to locate the flaws or debonds. Finally, a double-exposure hologram is obtained as a permanent holographic record of the observed flaw or debond. This hologram is based on the information obtained from the real-time search mode discussed above.

DISCUSSION OF RESULTS

Several hundred holograms were taken during the testing series of the positive pressure loading technique. The holographic results from three of the tests are shown in Figures 11, 12, and 13, which are photographs taken through the hologram.

Figure 11 displays some results of test sample plate 2, which was positioned in the sample holder with the fiberglass side facing outward. The hologram in the precision holder was taken while the plate was at a pressure of 5.5×10^3 dyne/cm^2 (2.5 psi). The interference pattern of Figure 11 was photographed after a pressure change of 1.1×10^3 dyne/cm^2 (0.5 psi). The figure depicts two distorted regions in an otherwise concentric elliptical fringe pattern. One is in the center of the left-hand side of the plate; the other distortions are the kinks observed in the lower right-hand corner. These distortions persisted when the pressure was increased. The first distorted region (to the left) coincided with the position of the programmed flaw of the grease fingerprints. The second distorted region (lower left) coincided with the location of the Teflon disc. As the pressure was lowered to 1.1×10^3 dyne/cm^2 (0.5 psi), the fringes appeared to completely surround the Teflon disc. This phenomenon is shown in Figure 12, which was photographed with the overhead lights off. Although a third flaw, the AF-32 plug, was said to be present in the right-hand corner, it was never observed on this plate. Also, throughout the testing using the positive pressure technique, no flaws were observed for plate 1. Figure 13 presents a photograph of the real-time fringes of plate 3. The reference pressure on the test plate was 6.6×10^4 dyne/cm^2 (30 psi), and the observed fringes were formed at the pressure of 6.76×10^4 dyne/cm^2 (30.375 psi). This fringe distortion in the right-hand corner essentially coincides with the position of the programmed flaw of the AF-32 plug. Incidentally, this flaw on this plate was persistent in some form of distortion over a wide range of pressure loading.

A similar procedure when applied to all three test plates with the ceramic side facing outward provided no observable distortions in an otherwise concentric fringe pattern.

In summary, with the pressure loading technique the following observations were made on the fiberglass side: two of the programmed flaws in plate 2, one programmed flaw in plate 3, and none in plate 1. No significant distortions of the fringes were observed on the ceramic side. Since all three kinds of flaws have been observed and since the system is highly sensitive to minute surface variations on the order of a quarter of a micron, the only explanation for its nondetection of all flaws on all plates is that these undetected flaws must have rebonded to the epoxy during the curing process. It has been learned subsequently from the test sample supplier that the rebonding probability does exist. The fact that no indications of any programmed flaws appeared on the ceramic side is probably because the ceramic material is both harder and many times thicker than the fiberglass. Efforts at higher pressures for the ceramic case proved negative since the ceramic tends to crack.

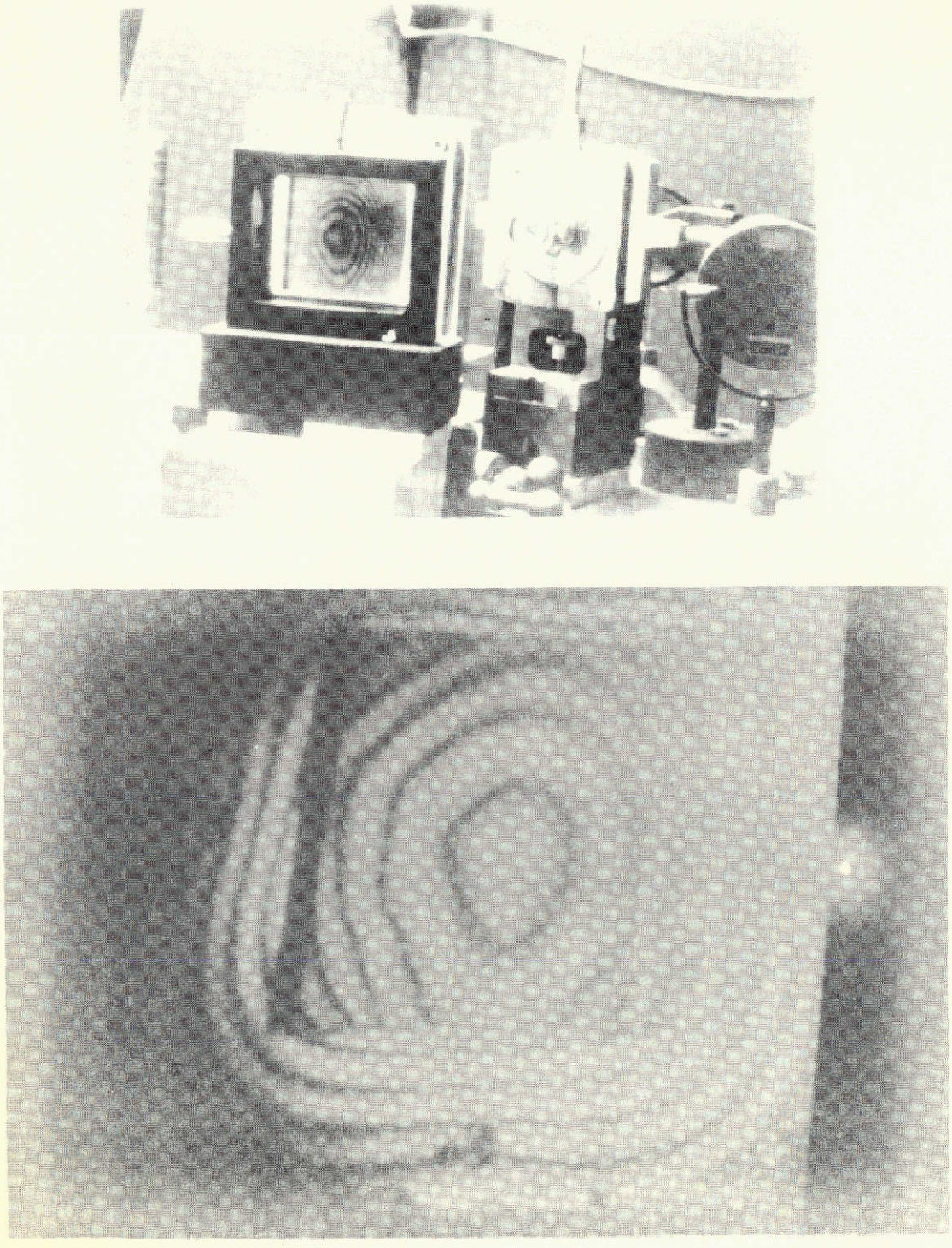

Figure 11. Real-time hologram of plate number 2,
$P = 1.1 \times 10^3$ dyne/cm^2 (0.5 psi).

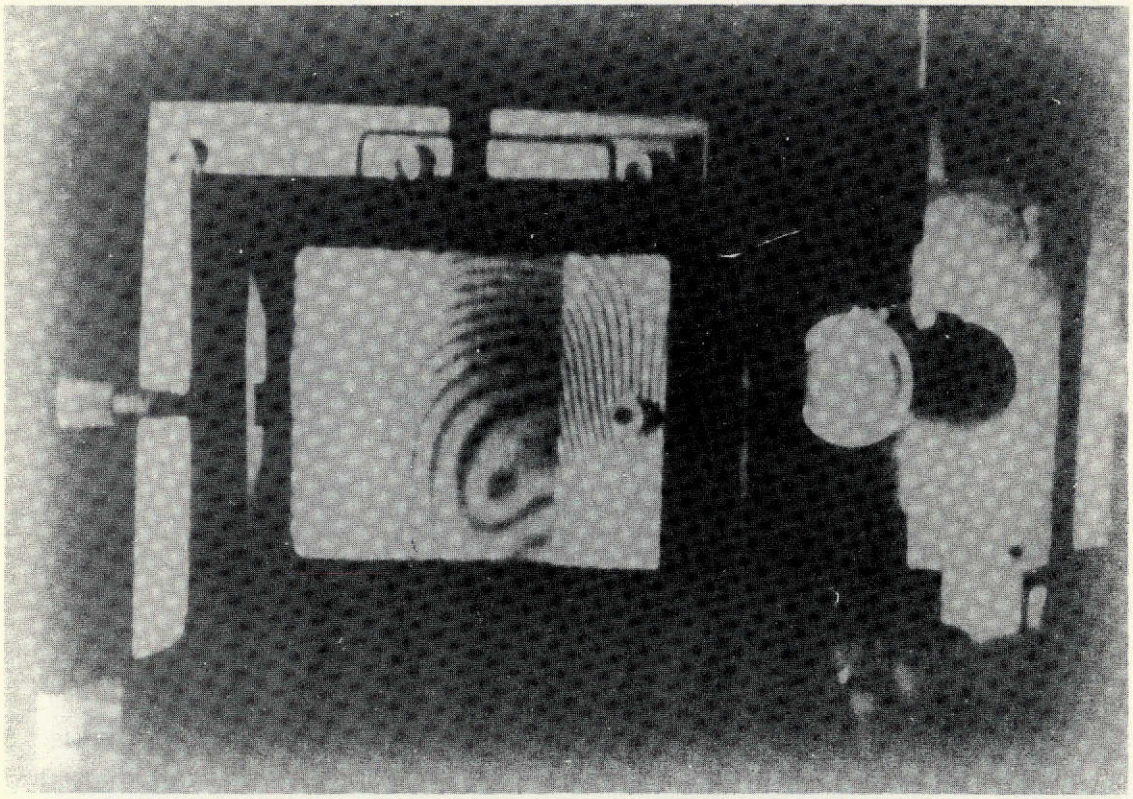

Figure 12. Real-time hologram of plate number 2, $P = 4.4 \times 10^3$ dyne/cm^2 (2.0 psi).

Thermal and vibration loading studies of these samples are presently under way, and the data are being analyzed. These different loading techniques are being employed to see if the flaws which failed to show up in the pressure loading tests will appear as a result of their different characteristics with regard to thermal conductivity and resonant frequencies.

George C. Marshall Space Flight Center
National Aeronautics and Space Administration
Marshall Space Flight Center, Alabama, October 1973
983-15-28-0000

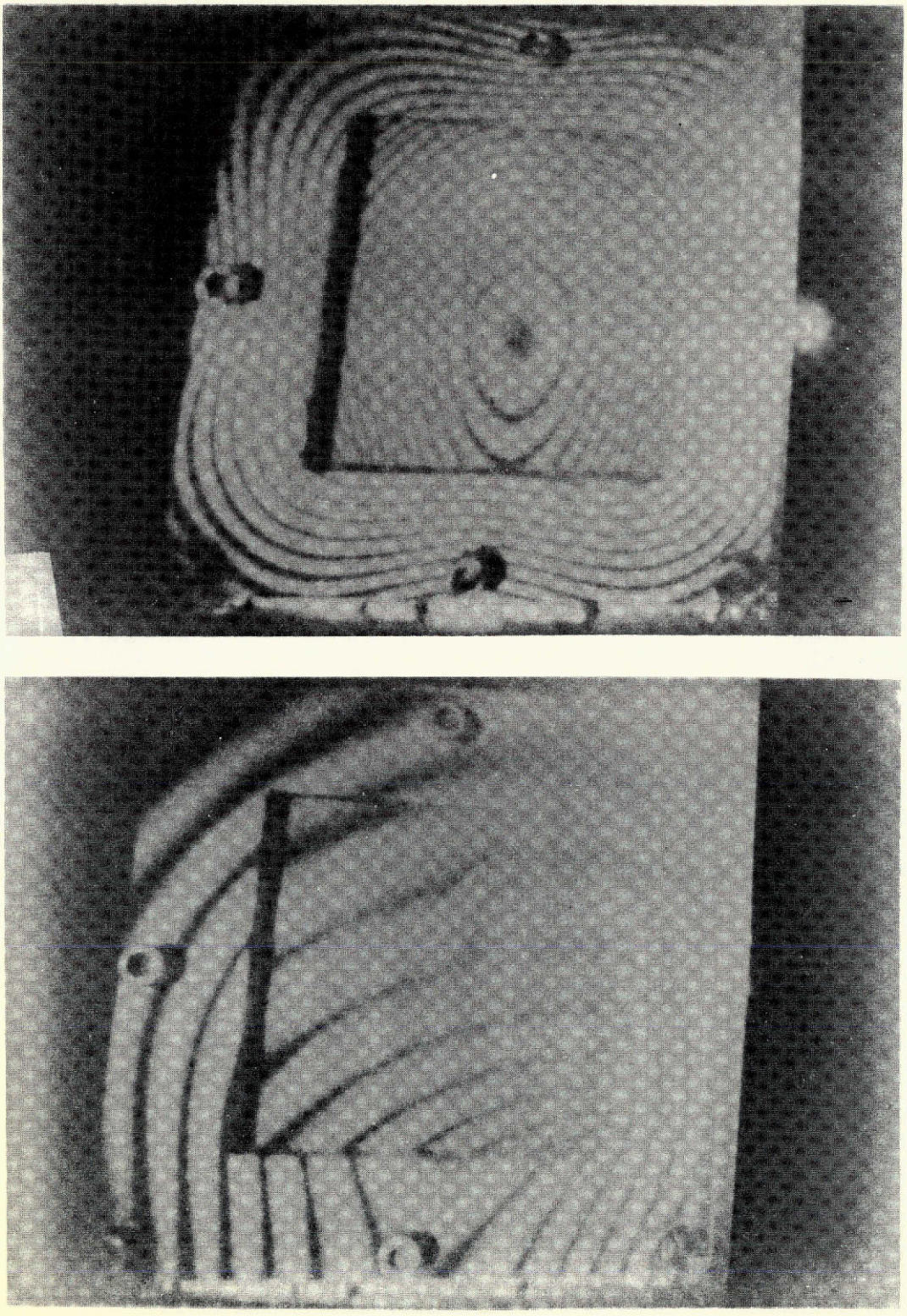

Figure 13. Real-time hologram of plate number 3,
$P = 6.76 \times 10^4$ dyne/cm^2 (30.375 psi).

REFERENCES

1. Schliekelmann, R.J.: Holographic Interference as a Means for Quality Determination of Adhesive Bonded Metal Joints. International Council of the Aeronautical Sciences, 8th Congress, Amsterdam, Netherlands, Aug. 28 – Sept. 2, 1972.

2. Aprahamian, R.: Some Useful Equations of Holography. TRW Systems Group Report No. AM 70-2, Jan. 1970.

BIBLIOGRAPHY

Chu, W.P.; Robinson, D.M.; and Goad, J.H.: Holographic Nondestructive Testing with Impact Excitation. App. Opt., vol. 11, July 1972, pp. 1644-1645.

Collier, Burckhardt, and Lin: Optical Holography. Academic Press, New York, 1971.

The Thermal and Mechanical Properties of Slip-Cast Fused Silica from 70°F to 2200°F. Final Report to Georgia Institute of Technology, Southern Research Institute.

Walton, J. D., Jr.: Radome Engineering Handbook. Marcel Dekker, Inc., New York, 1970, pp. 275-283.

NASA-Langley, 1974